Title
Spin-orbit torque induced magnetization switching in tungsten/ thulium iron garnet bilayer

Author
Zhang, Peng

Publication Date
2018

Peer reviewed|Thesis/dissertation

UNIVERSITY OF CALIFORNIA

Los Angeles

Spin-orbit torque induced magnetization switching in tungsten/ thulium iron garnet bilayer

A thesis submitted in partial satisfaction

of the requirements for the degree

Master of Science in Electrical & Computer Engineering

by

Peng Zhang

ABSTRACT OF THE THESIS

Spin-orbit torque induced magnetization switching in tungsten/ thulium iron garnet bilayer

by

Peng Zhang

Master of Science in Electrical & Computer Engineering

University of California, Los Angeles, 2018

Professor Kang Lung Wang, Chair

Magnetization switching by current-induced spin-orbit torque (SOT) is of great interest for its potential application in ultralow-power non-volatile memory devices. The past research on SOT based MRAM heavily relies on the spin-dependent transport in ferromagnetic (FM) conductors. However, such system has additional energy dissipation due to the Joule heating in the metallic FM layer. Moreover, the propagation length of spin current is limited by the short spin-diffusion length and the strong magnetic damping in FM metals. Magnetic insulators (MIs), attract tremendous interest for ultralow-power spintronics and spin wave application recently due to low Gilbert damping and absence of Ohmic loss. In this thesis, we achieved magnetic switching of an insulating magnetic ferrite thulium iron garnet (TmIG) by current-induced SOT in the nonmagnetic metal (NM) tungsten (W) layer. The switching current density is as low as 7.5×10^{10} A/m^2 for the W (5 nm)/TmIG (15 nm). Further thickness dependent study shows the SOT efficiency increases with the thickness of TmIG, which is in consistence with the theoretical proposed Ms-effect. This finding shed light on the understanding of SOT in MIs and promote the development of MI-based low-power spintronics.

The thesis of Peng Zhang is approved.

Chee Wei Wong

Chandra J Joshi

Kang Lung Wang, Committee Chair

University of California, Los Angeles

2018

TABLE OF CONTENTS

LIST OF FIGURES

ACKNOWLEDGMENTS

I would like to express my special thanks of gratitude to my advisor, Dr. Kang Wang, for his professional guidance and valuable support throughout this work. I also would like to thank Qiming Shao for guiding me to do the transport measurement and sharing data with me. At last, I would like to express my sincere appreciation to Professor Chee Wei Wong and Professor Chandrashekhar Joshi for their kindness of reviewing this thesis. It is a great honor for me to have them serve as my thesis committee.

CHAPTER 1

Introduction

1.1. Spintronics Overview

Moore's Law is the observation made by Intel co-founder Gordon Moore that the number of transistors on a chip doubles every year while the costs are halved. The industry indeed made so many innovations and kept following the prediction of Moore during the past half-decade. However, with the continuous scaling of MOSDET, modern electronics have approaching the dimension limit. Various short-channel effects arise including drain-induced barrier lowering (DIBL), gate induced drain leakage (GIDL), velocity saturation, and hot carrier effects, etc. [1][2][3]. These short-channel effects as well as electro-thermal heating problems, severely degrade the performance of modern electronic devices.

Extensive effort has been done by researchers to search for alternative method to keep or even go beyond the Moore's Law. These approaches include switch silicon to new materials such as III-V semiconductor and two-dimensional channel materials, and new structure design such as gate-all-around nanowire FETs [4]. However, those approaches are very hard to become real applications, due to the difficulty and cost for high throughput fabrications. Spintronics, which makes use of the spin degree of freedom of electrons, turns out to be very promising to be next-generation electronics. Spintronics focuses on the research of spin-dependent transport in solid states materials and devices.

With the coming of the big data era, there is increasing demand for data storage capability and computation ability, as well as lower energy cost. In traditional CMOS technology, memory devices include Static Random-Access Memory (SRAM), Dynamic Random-Access Memory (DRAM), and FLASH memory devices. SRAM has very high speed, but it has low integration density and high cost since each SRAM memory cell is comprised of 6 Transistors. DRAM has lower cost and high

integration density, but it needs extra power for continues refreshment because the information is stored by a capacitor. For Flash memory, although it is non-volatile, its writing speed is far behind SRAM and DRAM. Magnetic random-access memory (MRAM), as a non-volatile memory, which has the combined advantages of writing speed and writing energy, is becoming the most promising next generation memory devices.

1.2. GMR and TMR

The electrical read-out mechanism of a MRAM is based on magnetization dependent electrical transport properties. The most important and widely used phenomenon are giant magnetoresistance (GMR) and tunneling magnetoresistance (TMR).

1.2.1 GMR and spin-valve

Giant magnetoresistance (GMR) is a quantum mechanical magnetoresistance effect observed in multilayers composed of alternating ferromagnetic and non-magnetic conductive layers. The effect is observed as a significant change in the electrical resistance depending on whether the magnetization of adjacent ferromagnetic layers is in a parallel or an antiparallel alignment. The overall resistance is relatively low for parallel alignment and relatively high for antiparallel alignment. This phenomenon was first observed by Albert Fert and Peter Grünberg, and then they shared the 2007 Nobel Prize in Physics for the discovery of GMR [5].

After that, magnetic multilayer stacks have progressively brought spintronics into real life applications, which is later called spin valves. The typical structure of a spin valve is shown in figure 1-1. The simplest spin valve structure consists of a conducting non-magnetic material, sandwiched between two conducting ferromagnetic materials. One of the ferromagnetic material has large coercivity field and pinned magnetization, which is called fixed layer. Another one has smaller coercivity thus the magnetization can be switched upon applying a magnetic field of

appropriate strength, which is called free layer. As a result, it has two distinct states: a parallel, low-resistance state, and an antiparallel, high-resistance state. Making use of GMR effect, spin valves are widely used in magnetic sensors for reading data from hard drives, biosensors, MEMS and other devices. It is also widely used in MRAM as a unit for storing one-bit information.

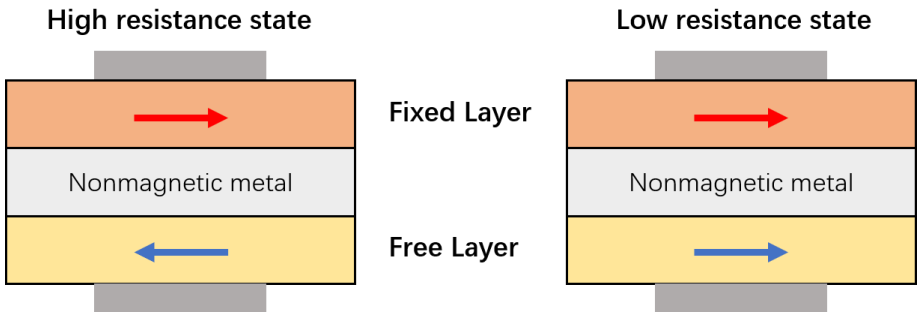

Figure 1-1. Spin valve structure: a conducting non-magnetic material sandwiched between two conducting ferromagnetic materials

1.2.2 TMR and MTJ

Very similar with GMR, the TMR is a magneto-resistive effect that occurs in a magnetic tunnel junction (MTJ), which is a component consisting of two ferromagnets separated by a thin insulator. The structure of a MTJ is similar with spin valve, except that the conducting nonmagnetic material (yellow region in figure 1-1) is replace by a nonmagnetic insulator. Since this process is forbidden in classical physics, the tunnel magnetoresistance is a strictly quantum mechanical phenomenon. TMR is discovered after GMR, and has much higher magnetoresistance ratio, so nowadays most magnetic reading sensors are made of MTJs.

1.3. Spin-transfer torque and spin-orbit torque

Having talked about the reading mechanisms in previous part, it is time to consider the writing mechanisms. The key to achieve low-power and high-speed operation of MRAMs is to have a fast

and energy-efficient magnetization switching of the free layer of the MTJs. In MTJs, the fixed layer is usually attached to an antiferromagnetic material, and the antiferromagnet could pin the magnetization state of an adjacent ferromagnetic layer through exchange bias. It can be understood as the effective coercivity is increased. So, if we apply a magnetic field weaker than the coercivity of fixed layer but stronger than the coercivity of free layer, the state of the MTJ can be effectively tuned.

However, in real memory device, by no means an external magnetic field should be applied to make the device working. We need magnetization manipulation by electric properties, such as current and voltage. As a result, widely used writing mechanism now is by current induced Oersted field. However, magnetization manipulation by current-induced Oersted field is very energy consuming and hard for high-density integration. On the contrary, spintronics approaches offers new approaches for fast and efficient magnetization switching.

1.3.1 Spin-orbit coupling (SOC)

The spin angular momentum of electron can interact with its orbital angular momentum. This lead to splitting of different energy levels which can lead to different transition energies. This effect is known as spin orbit coupling. In the classic description, the electron is moving at high speed through the radial electric field of the nucleus. On the other hand, in the electron coordinate, the nucleus is also circling around the electron, and this motion create an effective magnetic field which gives the electron a Lorentz force in the direction perpendicular to its motion and Zeeman energy. In other words, this magnetic field interacts with the electron's magnetic dipole moment to produce the spin-orbit coupling. From this simple model, we can also have an intuitive understanding that heavy atoms further up the periodic table with larger charge on the nucleus, will usually have stronger spin-orbit effect.

After taking the realistic modification to the classic model, it can be proved that the general Hamiltonian of spin-orbit coupling in non-inertial frame is given by [6]

$$\hat{H}_{SO} = \frac{\mathrm{h}}{4m^2c^2}(\nabla V \times \mathbf{p}) \cdot \boldsymbol{\sigma} \tag{1.1}$$

The spin-orbit coupling can be divided into two types in terms of symmetry dependence: one is symmetry-independent spin-orbit coupling, which stems from atomic orbitals and exists in all types of crystals [7]; while the other one is symmetry-dependent, which exists only in crystals without inversion symmetry [8]. In terms the origin of inversion asymmetry, the symmetry-dependent spin-orbit coupling can be further divided into Dresselhaus coupling [9] and Bychkov-Rashba coupling [10]. The Dresselhaus coupling is due to bulk inversion asymmetry (BIA) of the underlying crystal structure, while the Rashba coupling is related to structure inversion asymmetry (SIA) of the confining potential, such as hetero-structure, surface spin-orbit coupling, device with applying voltage and 2-D materials.

As we know, in a periodic crystal, the spin degeneracy of the electron and hole states is the combined effect of inversion symmetry in space and time. Both symmetry operations change the wave vector k into −k, but time inversion also flips the spin, which can be expressed as below

$$\begin{aligned} &\text{Time inversion symmetry: } E_{\pm}(\mathrm{k}) = E_{\mp}(-\mathrm{k}) \\ &\text{Space inversion symmetry: } E_{\pm}(\mathrm{k}) = E_{\pm}(-\mathrm{k}) \end{aligned} \tag{1.2}$$

Thus, combining both we have a two-fold degeneracy of the single particle energies, E+(k) = E−(k) [11]. In order to have spin polarized current, we must break the spin degeneracy of electron and hole states. As a result, either the time inversion symmetry (TIS) or the space inversion symmetry (SIS) should be broken. By applying magnetic field or introducing magnetism in the material, TIS can be broken, thus resulting spin polarized current. This is the physical origin of spin-transfer torque which will be discussed later. In SIS-broken materials, spin orbit coupling begins to play a role, and can produce a spin-orbit-torque (SOT) on adjacent ferromagnetic layer.

1.3.2 Magnetization dynamics

The Landau–Lifshitz–Gilbert (LLG) equation is a fundamental nonlinear evolution equation describing the precessional motion of magnetization M in a solid. However, to understand the current-induced magnetization dynamics in a single magnetic layer characterized by inversion asymmetry, the LLG equation should be modified by taking into consideration the spin-transfer torque (STT) terms and the spin-orbit interaction [12]. The modified equation, which is also known as the Landau–Lifshitz–Gilbert–Slonczewski (LLGS) equation can be written as

$$\frac{\partial \mathbf{m}}{\partial t} = -\gamma \mathbf{m} \times \mathbf{H}_{\text{eff}} + \alpha \mathbf{m} \times \frac{\partial \mathbf{m}}{\partial t} + \boldsymbol{\tau} \tag{1.3}$$

where m is a unit vector along the magnetization direction, γ is the gyromagnetic ratio $\gamma = g\mu_B/\hbar$, where μ_B is the Bohr magneton and g is the Lande g-factor, H_{eff} is an effective magnetic field determined by the external magnetic field as well as the exchange stiffness, dipole field and anisotropy field caused by the spin–orbit interaction, α is the Gilbert damping constant causing relaxation of the magnetization to its equilibrium orientation [13], and τ represents current-induced torque, which is the focus of our discussion. The current-induced torque can be expressed as

$$\boldsymbol{\tau} = \boldsymbol{\tau}_{\parallel} \frac{\mathbf{m} \times (\hat{x} \times \mathbf{m})}{|\hat{x} \times \mathbf{m}|} + \boldsymbol{\tau}_{\perp} \frac{\hat{x} \times \mathbf{m}}{|\hat{x} \times \mathbf{m}|} \tag{1.4}$$

where $\boldsymbol{\tau}_{\parallel}$ and $\boldsymbol{\tau}_{\perp}$ are driving torques, and $\hat{x}$ is the unit vector along the polarization of the current. Figure9 illustrates the magnetization dynamics described by LLGS equation. The first term on the right side of Eq. (1.4) is the field-like term leading to precession of the magnetization about the effective magnetic field direction. The second term leads to relaxation of the magnetization towards this field. The direction of the spin transfer torque is either parallel to the damping torque or antiparallel to it, depending on the sign of the current.

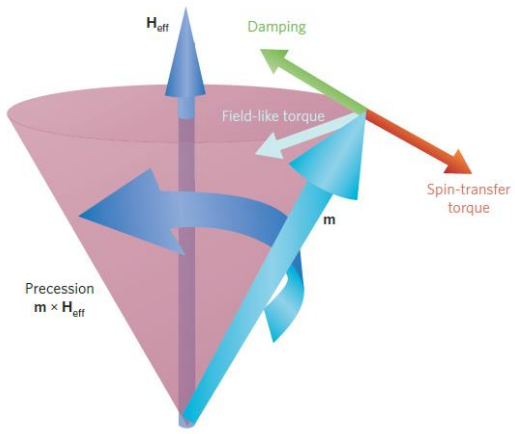

Figure1-2. Illustration of the LLGS dynamics (reprinted from [14]). The magnetization (m) precession about the effective field direction (H_{eff}). The green arrow illustrates the dissipative (damping) torque that tends to move the magnetization toward the effective field direction. The red arrow is the spin-transfer torque and the light-blue arrow is the effective field torque with an electron spin polarization collinear with the effective field.

1.3.3 Spin-transfer torque and STT-MRAM

The discovery of the possibility to manipulate and induce switching of the magnetization by spin-polarized currents via the spin transfer torque (STT) effect. Spin transfer torque is an effect in which the orientation of a magnetic layer in a magnetic tunnel junction or spin valve can be modified using a spin-polarized current. An electric current is generally unpolarized consisting of 50% spin-up and 50% spin-down electrons, while a spin polarized current is one with more electrons of either spin. The spin polarization current can be generated by passing the current through the “fixed layer”. If the spin polarized current is then directed into the “free layer”, the angular momentum of the electrons can be transferred to this layer, changing its magnetization orientation [15].

In the absence of any spin transfer torque or damping, if *m* is instantaneously tilted away from z-axis then it will precess in a circle, due to the torque from the applied magnetic field. If there is

damping but still no applied current, the torque due to damping will push *m* back toward the low-energy configuration along z-axis. When a current is applied, the situations are shown in Figure1-3. For current below a critical current, *m* spirals back toward the low-energy direction due to magnetic damping. For current larger than the critical value, the spin transfer torque causes M spiral away from z-axis and finally stay in either stable steady-state precession at large precession angle or magnetic reversal [15].

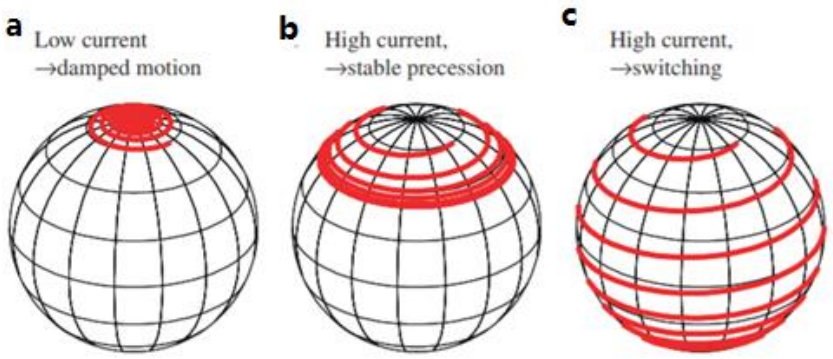

Figure1-3. Illustration of spin-torque-driven dynamics for the magnetization vector. (a) Damped motion under low current, and either stable precession (b) or switching (c) under large current. (figure reprinted from [15])

As shown in the above, the spin transfer torque offers an effective way to manipulate the magnetization of ferromagnets, which is very important in memory and logic spintronic application. However, conventionally that is realized through transferring spin angular momentum between a 'fixed' and a 'free' ferromagnetic layer separated by a non-magnetic spacer, and the dependence on a polarizer ferromagnetic layer largely confined its application.

The MRAM biased on STT writing mechanism is call STT-MRAM. Figure 1-4 (a) shows the typical structure of a 1 transistor—1 MTJ (1T-1R) STT-MRAM cell. The MTJ is composed of a bi-stable free layer and a pinned layer separated by a tunneling oxide. The read-out process is applying a smaller current and measure the voltage via the tunneling magnetoresistance (TMR) effect. The writing process is performed by passing a spin-polarized current, which transfers some of its

momentum to the “free layer”, inducing a torque that can result in switching depending on the direction of the current. When the current is from “fixed layer” to “free layer”, the transmitted spin polarized current writes the magnetization of “free layer” from antiparallel state to parallel state. When the current direction reverses, the spin polarized current reflected at the “fixed layer” write the “free layer” magnetization from parallel to antiparallel. The schematic of the STT writing process is shown in figure 1-4 (b) and (c).

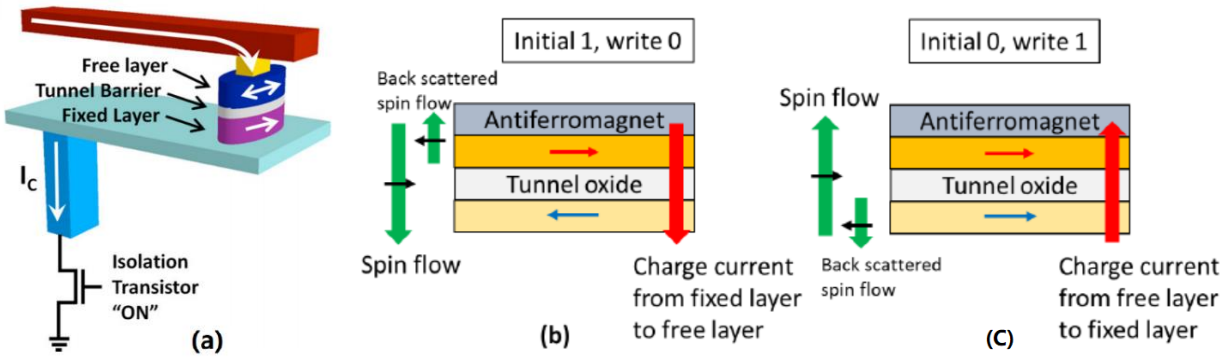

Figure 1-4. (a) the structure of a 1 transistor—1 MTJ (1T-1R) STT-MRAM cell (reprinted with permission from [16]. (b) STT writing mechanism from “1” (antiparallel) to “0” (parallel). (c) STT writing mechanism from “0” (parallel) to “1” (antiparallel)

1.3.4 Spin-orbit torque and SOT-MRAM

Although STT-RAM has the advantage of non-volatility, low writing power, and high speed, some shortcomings are still limiting the reliability and endurance of STT-MRAMs. First, the current density required for writing is very large thus can causing the damage of the MTJ barriers, especially when the writing time reaches nanosecond scale for high frequency applications. Second, since the writing current and reading current share the same path through the MTJ, it becomes more challenging to fulfill a reliable reading without ever causing switching at advanced technology nodes [17]. Third, the dependence on a polarizer ferromagnetic layer largely confined its applications. researchers have recently discovered some other alternative methods to generate

spin torque without a polarizer ferromagnetic layer and with separate writing and reading path [18]. These methods includs the spin Hall effect, Rashba and Dresselhaus effect. In these effects, the non-equilibrium spin accumulation due to spin-orbit coupling, could give rise to a torque on the magnetization. This phenomenon is also known as spin-orbit torque (SOT).

In materials with strong spin-orbit coupling, the spin degeneracy of electrons and holes is broken, so the conducting electrons of holes would experience an effective magnetic field from SOC. As a result, when the current is passing through, part of the conducting current would be converted into a net spin current in the transverse direction. The spin polarization direction, conducting current, and spin current direction are perpendicular with each other. In this phenomenon, a perpendicular spin current is generated through a conducting current, which is also called Spin Hall Effect (SHE). From the experimental perspectives, many experimentalists have been working to experimentally demonstrate and quantitatively measure the SHE in different materials, including semiconductors like GaAs [19] and ZnSe [20] and heavy metals like Ta, W, and Pt [21]. The SHE is especially pronounced in heavy metal materials, and many researchers have been working on the spintronic application of SHE on heavy metal recently. In materials with broken space inversion symmetry as discussed in SOC section, Edelstein-Rashba SOC would also result in the conduction current to spin current conversion, and thus producing SOT. In contrary to the bulk spin hall effect, Rashba SOT usually happens in the two-dimensional surface or interfaces. Recent years, the study of Rashba SOT is usually in the metal system, interface of complex oxide, 2D materials, topological insulators, and antiferromagnetic materials.

The schematic of SOT induced perpendicular magnetization switching through an in-plane current is shown in figure 1-5. In the heterostructure of a ferromagnetic layer (FM) and nonmagnetic heavy metal layer (HM), the in-plane conducting longitudinal current would generates a perpendicular spin current, with the spin polarization along transverse direction. The spin-polarized current was injected into the FM layer and interacts (angular momentum exchange) with the local magnetization (usually the 3d or 4f electrons of the FM), thus producing an effective SOT field

onto the FM layer. The direction of the effective SOT field is along the cross product of spin polarization and magnetization ($\vec{\sigma} \times \vec{m}$), which is indicated as the red dashed line in figure 1-5. If a small external magnetic field is applied to the FM layer with perpendicular anisotropy (PMA), the magnetization would be tilted by a small angle. As a result, the SOT effective field would have a perpendicular component. If the SOT field is strong enough, the magnetization could be switched. For a current with reverse direction, the switching direction would also be reversed.

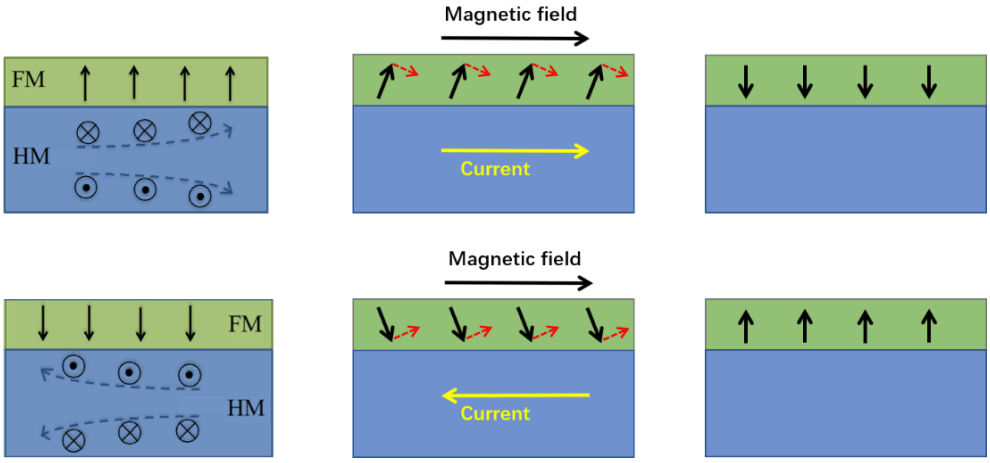

Figure 1-5. SOT writing mechanism of the HM/FM bi-layer. The yellow arrow indicated currents flow direction, and red dashed arrow show the direction of SOT effective field.

The MRAM biased on SOT writing mechanism is call SOT-MRAM. Figure 1-6 (a) shows the typical three-terminal structure of a SOT-MRAM cell, whose read-out process is based on TMR and writing based on SOT. Compared to spin transfer torque, spin-orbit torque has several advantages regarding the switching efficiency, power consumption, switching speed and scalability. Spin-orbit torque-based devices have become the research hot spot in recent years, which has very promising application prospects in novel spintronic memory and logic devices. In 2011, Miron I. M. et al [22] demonstrated switching of a perpendicularly magnetized cobalt dot driven by in-plane current injection at room temperature, as shown in figure 1-6 (b).

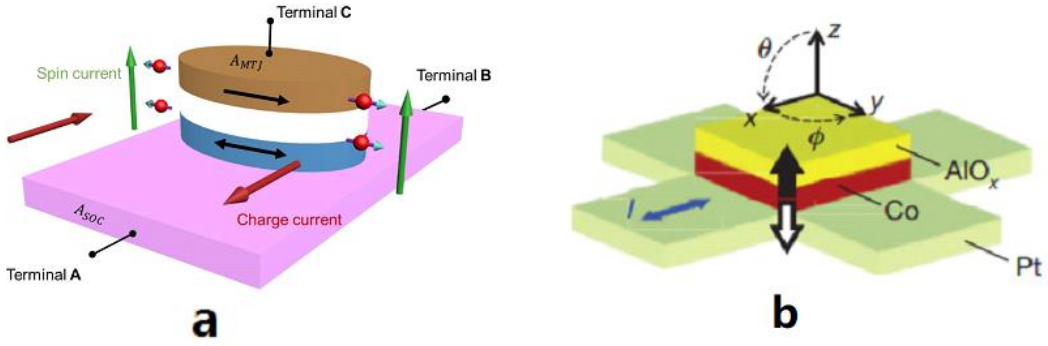

Figure 1-6. (a) the structure of a SOT-MRAM. (b) Device schematic and current-induced switching [22].

1.4 Hall Resistance

The Hall measurement is very important for quantitatively determining the transport properties of semiconductors, such as carrier density and Hall mobility. The schematic of a hall bar set-up is drawn in Figure 1-7. The current is along the ±y direction, and the direction of external magnetic field is described by two angles: polar angle θ and azimuthal angle φ. Magnetoresistance and Hall resistance are measured using a four-probe technique.

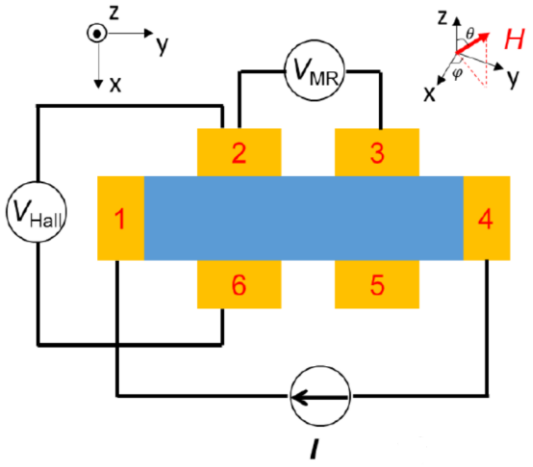

Figure 1-7. schematic of a Hall bar structure for electrical transport measurement.

For magnetic materials, when the magnetic field is applied perpendicular to the film plane, the general expression is given by [23]

$$R_{\mathrm{Hall}} = R_{\mathrm{OHE}} + R_{\mathrm{AHE}} = R_{\mathrm{O}} H_{\mathrm{Z}} + R_{\mathrm{A}} m_{\mathrm{z}} \tag{1.5}$$

Where R_{OHE} and R_{AHE} are the ordinary Hall Effect (OHE) resistance and Anomalous Hall Effect (AHE) resistance, respectively. H_{Z} is perpendicular magnetic field and m_{z} is perpendicular component of magnetization. For a nonmagnetic material, m_{z} is zero thus the $R_{\mathrm{Hall}} - H$ curve shows a linear relationship. Form the $\mathrm{V_{Hall}}$ and $\mathrm{V_{MR}}$ measurement, we can further obtain the carrier type, carrier density and its mobility. For ferromagnetic materials, the $R_{\mathrm{Hall}} - H$ curve will develop a hysteresis loop due to the ferromagnetic phase. When the magnetic field applied has in-plane components, the Hall resistance will have a component originated from planar Hall Effect (PHE), which has the same origin with the anisotropic magnetoresistance (AMR). Typically, the planar Hall resistance can be expressed by $R_{\mathrm{PHE}} = R_{\mathrm{P}} m_{\mathrm{x}} m_{\mathrm{y}}$, where R_{P} is the PHE coefficient, m_{x} and m_{y} are the magnetization component along x and y directions, respectively. As a result, the expression for Hall resistance should be modified as

$$R_{\mathrm{Hall}} = R_{\mathrm{OHE}} + R_{\mathrm{AHE}} + R_{\mathrm{AHE}} = R_{\mathrm{O}} H_{\mathrm{Z}} + R_{\mathrm{A}} m_{\mathrm{z}} + R_{\mathrm{P}} m_x m_y \tag{1.6}$$

1.5 Thesis Outline

In chapter 2, we will discuss the spin transport properties of magnetic insulators (MI) thulium iron garnet (TmIG) and heavy metal (HM) tungsten (W) heterostructures, and further discuss the mechanism of the anomalous hall effect and spin-orbit torque in the HM/MI bilayer system. In chapter 3, we measured the SOT efficiency in TmIG/W bilayer, and achieved efficient magnetic switching of TmIG by current-induced SOT in tungsten (W) layer with very low critical current density. Further thickness dependent study shows the SOT efficiency increases with the thickness of TmIG, which is in consistence with the theoretical proposed Ms-effect. In chapter 4, we briefly summarize all important things discussed above and give a perspective of next steps in TmIG/W study.

CHAPTER 2

Spin Transport of Magnetic Insulators and Heavy Metal Heterostructures

The interplay between heavy metals (HMs) and magnetic insulators (MIs) in heavy metal/magnetic insulator (HM/MI) bilayer systems has attracted tremendous attention from both fundamental research and practical applications. Compared to the HM/FM bilayer system, where the FM is usually conducting materials, insulating magnetic materials has some special advantages. First, the HM/MI bilayer benefits from the low Gilbert damping in Mis, thus has wide applications in ultrafast spin dynamics. Second, different from magnetic metal cases, MIs only allow spin information to propagate through magnons, instead of itinerant electrons. The absence of Ohmic loss from the magnetic layer makes HM/MI bilayers more energy efficient than HM/magnetic metal cases. Interestingly, although conduction electrons in HM cannot pass across the interface into the MI layer, the spin current can still penetrate the interface via the s-d exchange interaction, which also gives rise to SOT. As a result, the HM/MI system offers wide opportunities for low-power ultra-fast spintronics.

2.1 Magnetic insulators

2.1.1 Structure and properties of RIG

Among a variety of magnetic insulator materials, rare earth iron garnet (RIG) family has attracted the most attention for their unique spin dynamic and magneto-optical properties since 1960s. Compared with other magnetic insulators, such as EuS and EuO, RIG family has a high Curie temperature (~550 K) and a large band gap. Figure 2-1 (a) shows the structure of rare earth iron garnets, which are cubic crystals with a chemical formula $R_3Fe_2Fe_3O_{12}$. It has two octahedral sites

and three tetrahedral sites occupied by Fe, and three dodecahedral sites occupied by Rear earth atoms [24].

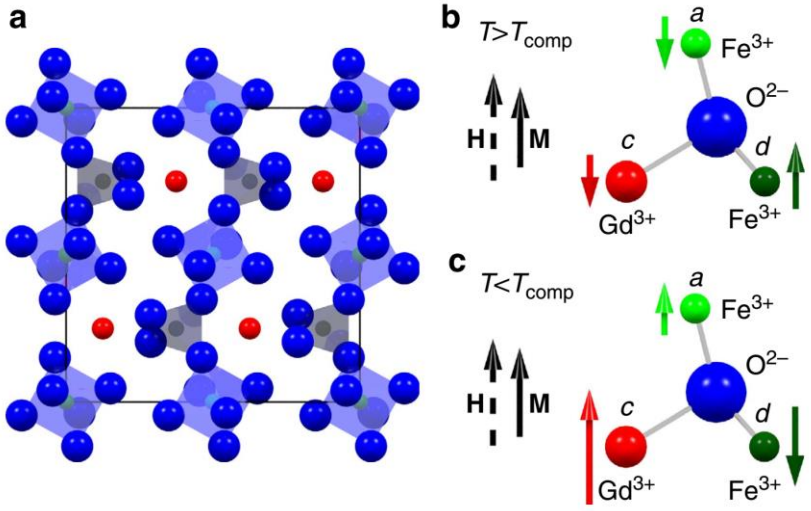

Figure 2-1. (a) structure of RIG. (b) and (c) magnetization configurations of two sublattice above and below magnetization compensation temperature a magnetic field. (figure reprinted from [24])

As shown in figure 2-1 (b), the two octahedral Fe (a site) and three tetrahedral Fe (d site) are antiferromagnetic coupled, and the magnetization of rear earth atom (c site) is antiferromagnetic coupled to the net magnetization of the iron atoms, namely antiparallel with the magnetization of tetrahedral Fe. It is obvious that RIG consists of two antiferromagnetic coupled sublattices, so it is a ferrimagnetic material. Usually there is a magnetization compensation temperature T_{comp} where the magnetization of each sublattice canceled out with each other. Above T_{comp} the Iron sublattice dominants, while below T_{comp} the rear earth sublattice dominant. When emerged in a magnetic field, the total magnetization will be aligned with magnetic field, resulting two different magnetization configurations at high and low temperature, as shown in figure 2-1 (b) and (c).

2.1.2 Magnetic characterization of TmIG

To access SOT and realize current induced magnetization switching (CIMS), we prepare high-

quality TmIG thin films with different thickness t_{TmIG} and characterize their magnetic properties. The TmIG film is grown on $Nd_3Ga_5O_{12}$ substrate by pulsed laser deposition. The sufficiently tensile strain induced by large lattice mismatch between TmIG and underlying substrate enables robust perpendicular magnetic anisotropy (PMA) for TmIG films [25]. Atomic force microscopy image (figure 2-2 a) shows that the TmIG thin films has an atomically flat surface with mean roughness as low as 0.1 nm, providing a sharp interface for efficient spin momentum transfer. Figure 2-2 (b) and (c) shows the magnetic moment as a function of an out-of-plane field measured by superconducting quantum interference device (SQUID) at room temperature, and the square shape hysteresis loop indicates the TmIG has perpendicular anisotropy. We measured total magnetic moment as a function of temperature for different TmIG thicknesses, and all these samples shows Curie temperature far above room temperature.

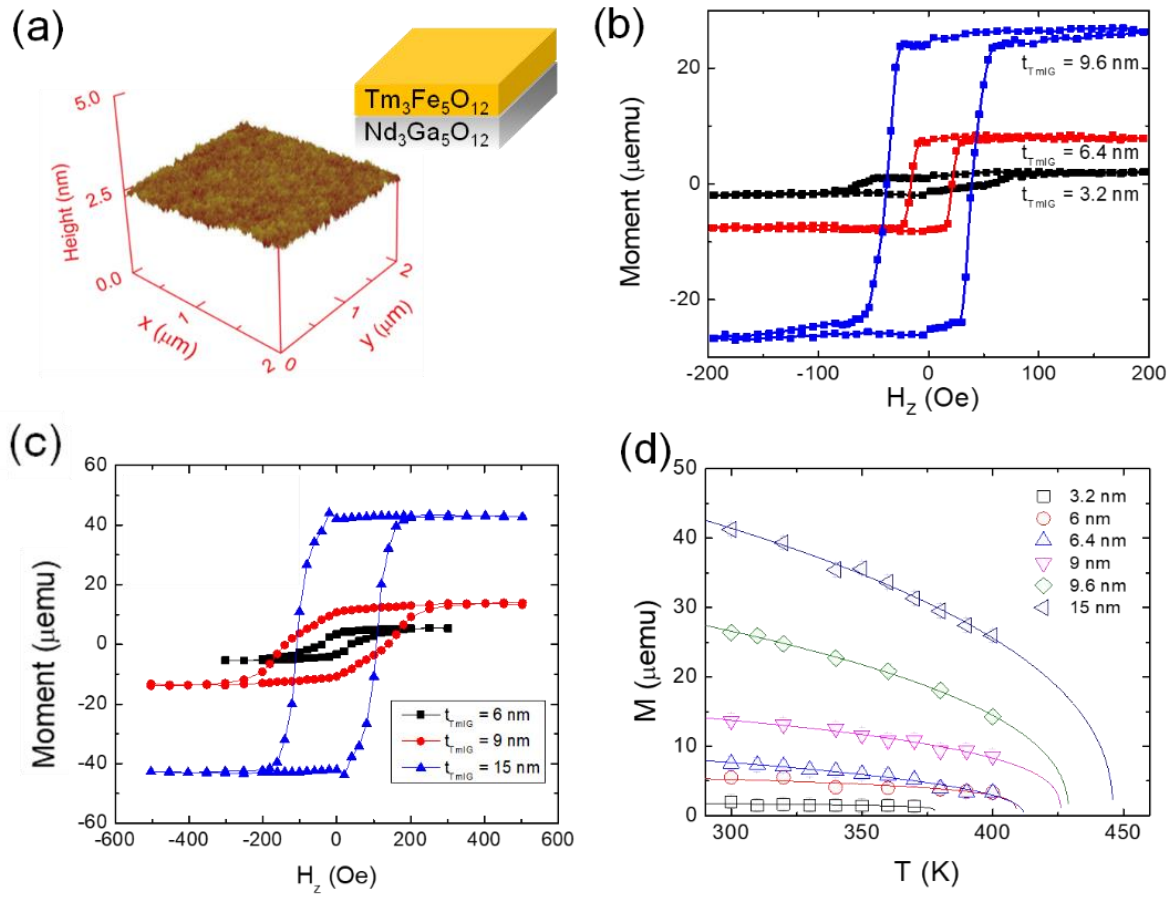

Figure 2-2. (a) Atomic force microscopy image of a 10 nm-thick TmIG film. (b) and (c) Magnetic moment as a function of an out-of-plane magnetic fields for TmIG thin films with different thicknesses at room temperature. (d) Total magnetic moment as a function of temperature for different TmIG thicknesses. The solid lines are power-law fits to $M = M_0\left(1-T/T_C\right)^{\beta}$. The nominal thin film area is 5 × 5 mm².

We observe a significant reduction of M_S with decreasing film thickness from a value close to the bulk M_S at 9.6 nm. This thickness-dependent M_S in TmIG thin films provides a unique platform to test the M_S dependent SOT, which was theoretically predicted to increase with M_S [26].

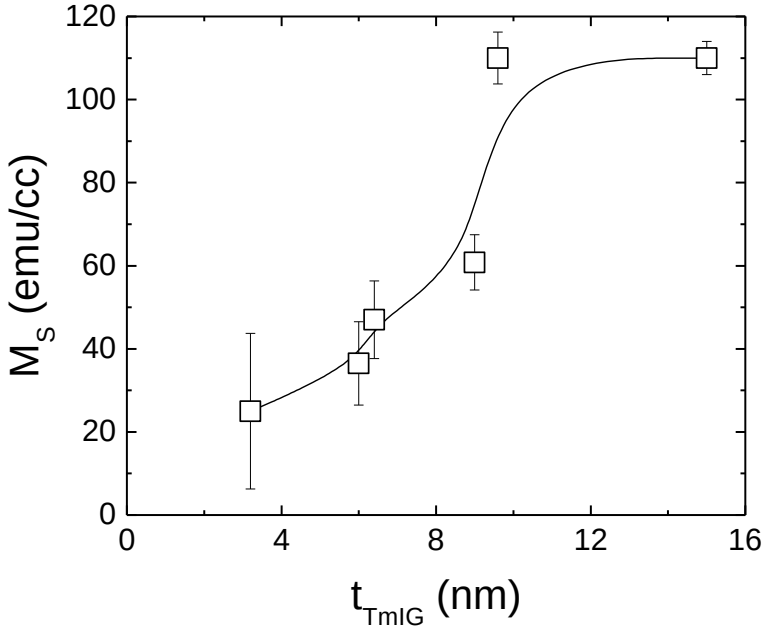

Figure 2-3. Saturation magnetization as a function of TmIG thickness at room temperature

2.2 Magneto-transport in TmIG/W bilayers

After sputtering 5nm tungsten layer on top, we fabricate W(5nm)/TmIG(t_{TmIG}) thin films into Hall bar devices (Figure 2-4a) for magneto-transport measurement. The anomalous Hall resistance

(AHR) in the W/TmIG is accurately determined by the sharp anomalous Hall hysteresis at low fields (Figure 2-4b). The transverse planar Hall resistance (PHR) is measured by rotating the magnetization in the xy-plane (Figure 2c). The spin Hall magnetoresistance (SMR) is measured with the increasing magnetic field along x direction. For the 9.6nm thick TmIG sample, it shows a R_{AHE} = 18Ω, R_{PHE} = 35Ωand R_{SMR} = 90Ω.

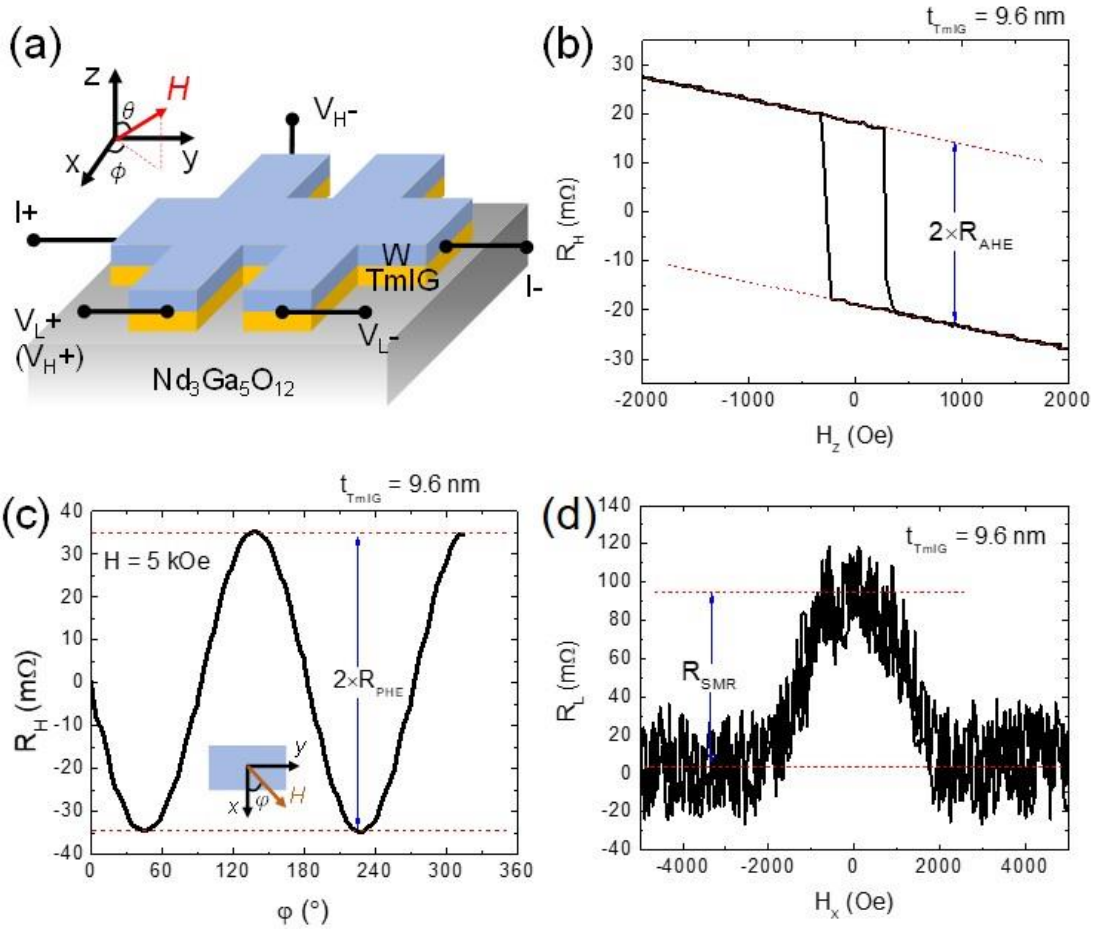

Figure 2-4 (a) Experimental setup for measuring resistance, spin torque and current-induced switching. (b) Hall resistance as a function of an out-of-plane magnetic field in the W(5 nm)/TmIG(9.6 nm). (c) Hall resistance as a function of a rotating in-plane constant magnetic field (5 kOe) for the W (5 nm)/TmIG(9.6 nm), where SMR-induced PHE is observed. (d) Longitudinal resistance as a function of an external magnetic field along the ±x direction in the W (5 nm)/TmIG (9.6 nm).

The popular explanation for observed AHE, PHE, and SMR in nonmagnetic metal and ferromagnetic insulator bilayer includes magnetization proximity effect, and spin current effect [27][28]. According to the SMR theory [28], the observation of sizeable AHR and PHR (SMR) indicates that there is a significant spin current being transmitted across the W/TmIG interface or a sizable spin mixing conductance.

CHAPTER 3

Spin-orbit Torque induced Magnetization Switching

3.1 Spin-orbit Torque Measurement

3.1.1 Second-harmonic Method

To examine the spin-orbit torque efficiency in W/TmIG bilayers, we quantify both damping-like torque efficiency ξ_{DL} and field-like torque efficiency ξ_{FL} by using the second-harmonic analysis of both anomalous and planar Hall. In second-harmonic measurement, we apply an AC current with frequency (ω) along longitudinal (y) direction, and measure the second harmonic (2ω) Hall voltage using lock-in technique.

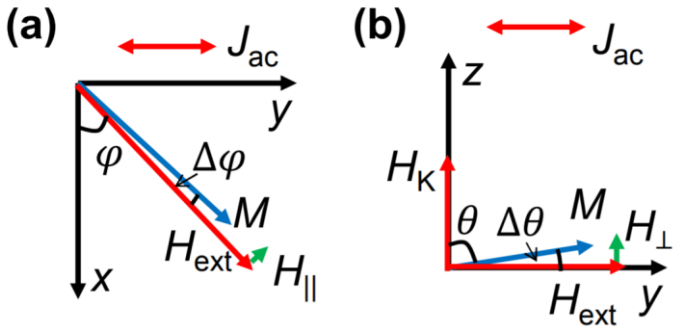

Figure 3-1 Illustrations of the magnetization vector under the AC current (ω) induced in-plane (a) and out-of-plane (b) spin-orbit effective fields

The Hall resistance without ordinary Hall effect is given by

$$R_{Hall} = R_{AHE} + R_{AHE} = R_A \cos\theta + R_P \sin^2\theta \sin\varphi \cos\varphi \tag{3.1}$$

where θ and φ are the polar and azimuthal angles for the magnetization. When the magnetization is dragged into the film plane ($\theta \approx 90°$) by a large magnetic field, and in the meantime a small AC

current is applied, the magnetization direction will deviate and oscillates around the equilibrium position. The deviation amplitude under the (field-like) in-plane SOT field is $\triangle\varphi$, and under the (damping-like) out-of-plane SOT field is $\triangle\theta$ as shown in Figure 3-1.

$$\Delta\theta(t) = \frac{H_{DL\perp}\sin\varphi\sin\omega t}{H_{\text{ext}} - H_{\text{K}}} \quad , \quad \Delta\varphi(t) = \frac{H_{\text{FL}\parallel}\sin\varphi\sin\omega t}{H_{\text{ext}}} \tag{3.2}$$

where H_{ext} is the external magnetic field, H_{K} is the out-of-plane anisotropy field, $H_{\text{DL}\perp}\sin\varphi$ comes from the cross product of magnetization and spin polarization, and $H_{\text{FL}||}\sin\varphi$ represents the component of the $H_{\text{FL}||}$ that is perpendicular to magnetization. Finally, the second-harmonic Hall resistance ($R_H^{2\omega}$) in a single domain subjected to an in-plane magnetic field can be written as [29]

$$R_{\text{H}}^{2\omega} = R_{\text{FL}}^{2\omega}\cos 2\varphi\sin\varphi + R_{\text{DL}}^{2\omega}\sin\varphi = R_{\text{PHE}}\frac{H_{\text{FL}}}{|H_{\text{ext}}|}\cos 2\varphi\sin\varphi + \frac{R_{\text{AHE}}}{2}\frac{H_{\text{DL}}}{|H_{\text{ext}}| - H_{\text{K}}}\sin\varphi \tag{3.3}$$

By applying a large constant in-plane magnetic field along different directions, we measure the second harmonic Hall signal. Then by fitting the $R_H^{2\omega}$ with the above equation, we can get separate the PHE component and AHE component (figure 3-2 a). Then we change the magnitude of the magnetic field and repeat the rotation angle measurement and fitting. Finally, by fitting the AHE component obtained at various magnetic field to $1/|H_{\text{ext}}\text{-}H_{\text{K}}|$, we can finally get the damping-like SOT effective field (figure 3-2 b). Similarly, by fitting the PHE component to $1/|H_{\text{ext}}|$, we can get the field-like SOT effective field. The damping like SOT field, which has large out of plan component, is the key for current induced magnetization switching. In the following measurement, our discussion is mainly focused on the damping like SOT efficiency. The damping like SOT efficiency ξ_{DL} can be calculated from $\xi_{\text{DL}} = \frac{2eM_{\text{S}}t_{\text{TmIG}}H_{\text{DL}}}{\hbar J_{\text{ac}}}$ [30], where e is the electron charge, $\hbar$ is the reduced Planck constant and J_{ac} is the applied current density. We observe a characteristic increase of ξ_{DL} as t_{TmIG} increases with a saturation length around 10 nm (see Figure 3-2c). Similarly, previous experiments have revealed that saturation magnetization increases and the saturated

around T_{mIG}=10nm.

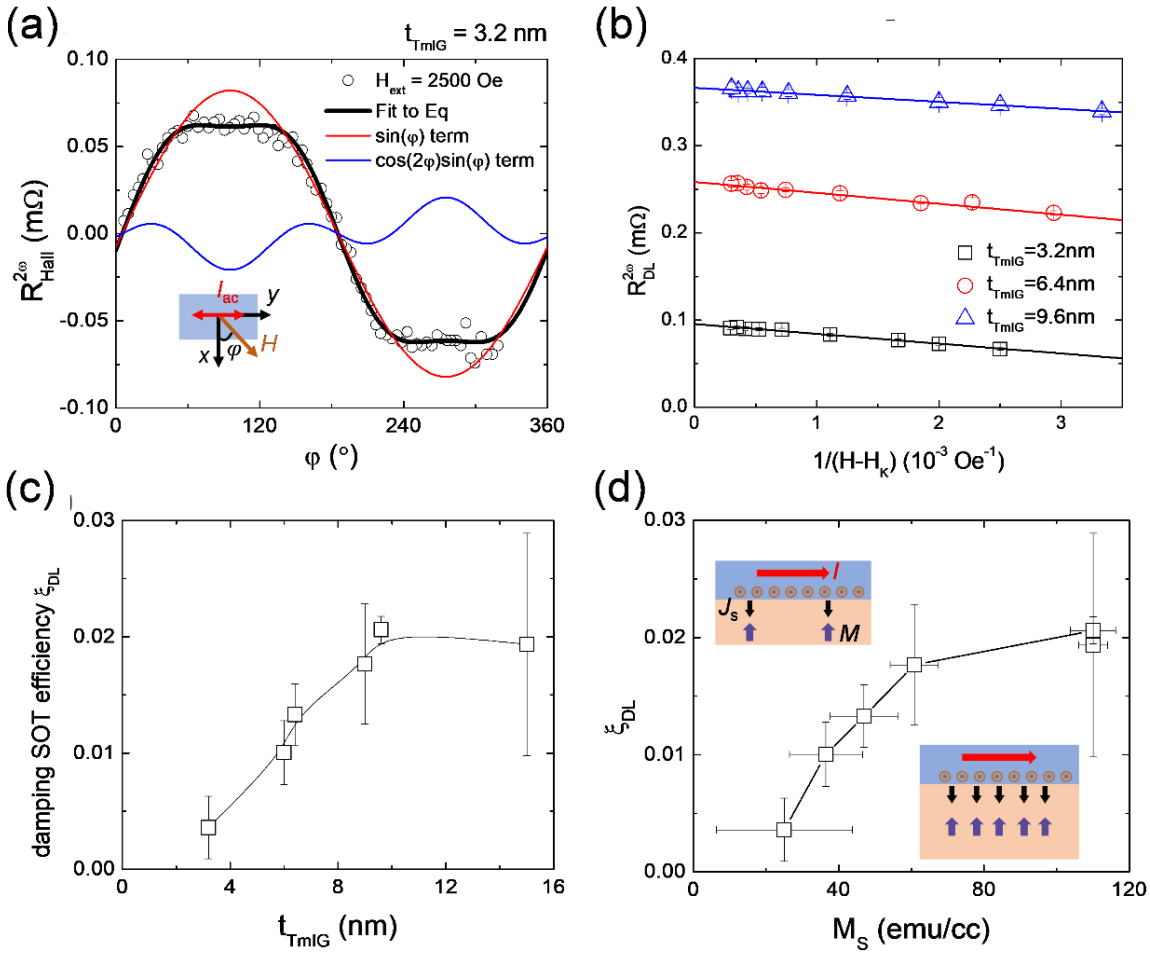

Figure 3-2. (a) Second-harmonic Hall resistance as a function of in-plane azimuthal angle for the external magnetic field 2500 Oe for the W (5 nm)/TmIG (3.2 nm), where the black curve is the fit to Eq. (1). Both cos2φsinφ (blue curve) and sinφ (red curve) angle dependencies are revealed. (b) Extracted damping-like torque contribution as a function of the inverse of external magnetic field subtracting the anisotropy field. The large intercepts are the spin Seebeck resistance. (c) Damping-like spin-orbit torque efficiency as a function of TmIG thickness. (d) Theoretical understanding of role of thermal fluctuation on the ξ_{DL} as a function of TmIG M_S.

Here, we discuss the mechanism for the TmIG thickness dependence of ξ_{DL}. We plot ξ_{DL} as a

function of saturated magnetization, and it shows that ξ_{DL} strongly depends on M_S, which we referred as M_S-effect. This M_S-effect has been theatrically proposed but has not been experimentally reported yet. In the perturbative treatment, the spin current absorbed by the ferromagnet can be obtained up to second order in the exchange interaction to yield the damping-like spin-orbit torque with $\xi_{DL}^2 \sim m_S^2$ [31]. As shown in figure 3-2d, when the M_S is small, ξ_{DL} is proportional to the M_S squared. Insets show two cases: in the left inset, the magnetic moment density is small and thus the number of spin channels is small, resulting in a small spin current injection; in the right inset, the magnetic moment density is large and thus the number of spin channels is large, resulting in a large spin current injection.

3.1.2 Loop-shift Method

To further support the observation of M_S-dependent ξ_{DL}, we perform the current-induced hysteresis loop shift measurement to independently determine ξ_{DL} [32]. In this method, we characterize the out of plan damping like SOT effective field by measure the perpendicular magnetic hysteresis loop shift, rather than through second harmonic Hall measurement. The mechanism is illustrated in figure 3-3. When applied a longitudinal DC current, there would emerge a perpendicular damping-like SOT field. Then swipe a smaller perpendicular magnetic field, we could expect the SOT field would either assist or block the perpendicular field induced magnetization switching. As a result, by applying DC current along opposite direction, we would expect the hysteresis loop shift in the opposite direction.

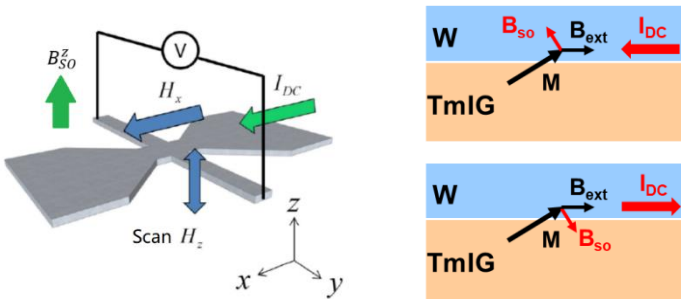

Figure 3-3 schematic of the loop-shift method for damping like SOT field measurement.

The results are shown in figure 3-2. We can see that the loop shift method qualitatively reproduces the results from the second-harmonic measurement as shown in figure 3-2. The consistency strongly suggests the existence of the M_S-effect on ξ_{DL}.

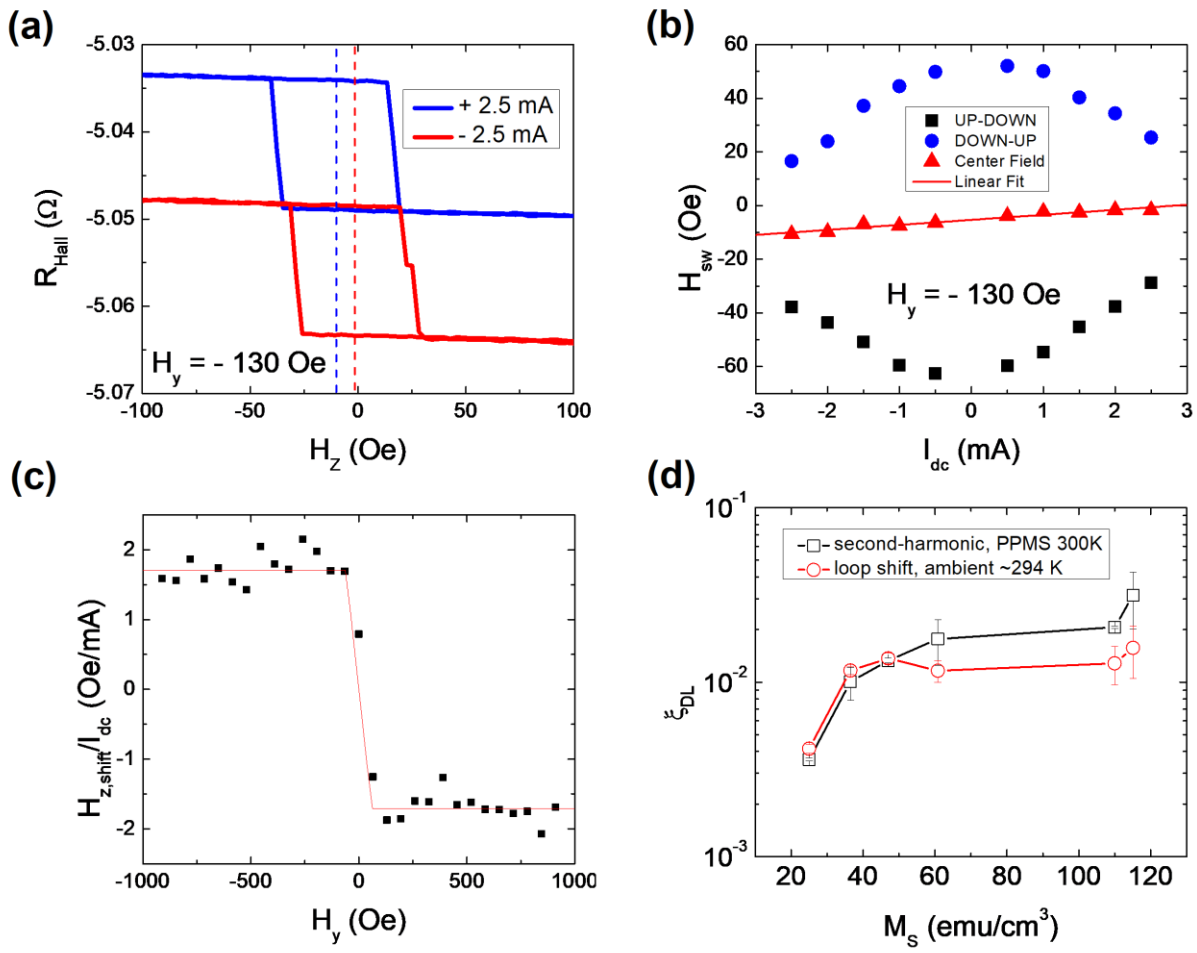

Figure 3-4. Determination of damping-like torque efficiency using the current-induced hysteresis loop shift method at room temperature. (a) Out-of-plane Hall hysteresis loops of W/TmIG(3.2nm) at Idc = + 2.5 mA and -2.5 mA with an in-plane external field Hy = -130 Oe applied. (b) Switching fields as a function of Idc with Hy = -130 Oe. (c) Out-of-plane hysteresis loop shift per mA as a function of the in-plane external magnetic field along the ± y direction. (d) Determined damping-like torque efficiency as a function of MS. The results from the second-harmonic method are shown as a comparison.

3.2 SOT Switching

After quantifying the spin torque efficiency, we perform the current-induced magnetization switching experiments for W/TmIG bilayers with different t_{TmIG}. Obviously, the ultimate goal of enhancing SOT efficiency through material and structure optimization, is to realize energy-efficient high-speed magnetization switching. The switching experiment is carried out with an external field along the current direction, and the switching is done by applying a 5 ms pulse with varying current amplitude, while the readout of magnetization status is through AHE.

The switching curve with the assistance of an in-plane magnetic field is shown in figure 3-5a, and the whole switching phase diagram is obtained by mapping the switching curve measured under various in-plane field (figure 3-5b). The switching direction is consistent with the sign of spin Hall angle of W and is opposite to the Pt/TmIG case [33]. We notice that the switching current is as low as ~3.5 × 10^{10} A/m² in the W(5 nm)/TmIG(6 nm) with the assistance of an in-plane magnetic field of only 135 Oe. This switching current is five times smaller than the Pt(5 nm)/TmIG(8 nm) case [33].

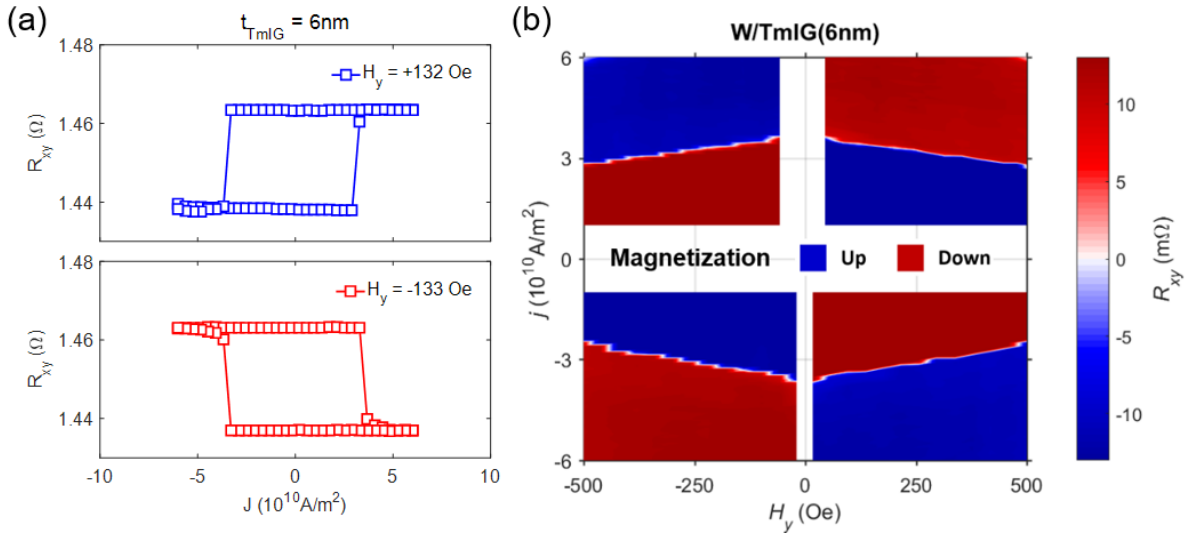

Figure 3-5 (a) Current-induced magnetization switching in W/TmIG with t_{TmIG}=6nm, where the external

field is along the current direction. (b) Switching phase diagram.

The switching is achieved in all W/TmIG sample with TmIG thicknesses ranging from 3.2nm up to 15nm (figure 3-6). The switching phase diagrams are also measured for all these samples, shown in figure 3-7. It is shown that even for the 15nm thick TmIG, the switching current is as low as 7.5 × 10^{10} A/m², which is still two times smaller than the Pt(5 nm)/TmIG(8 nm) case reported in [33]. This can be partially understood from a larger damping-like torque efficiency ξ_{DL} (~ 0.02) in the W/TmIG compared with the value (~ 0.01) in Pt/TmIG. This suggests that the large spin Hall angle in W enables more energy efficient magnetization switching.

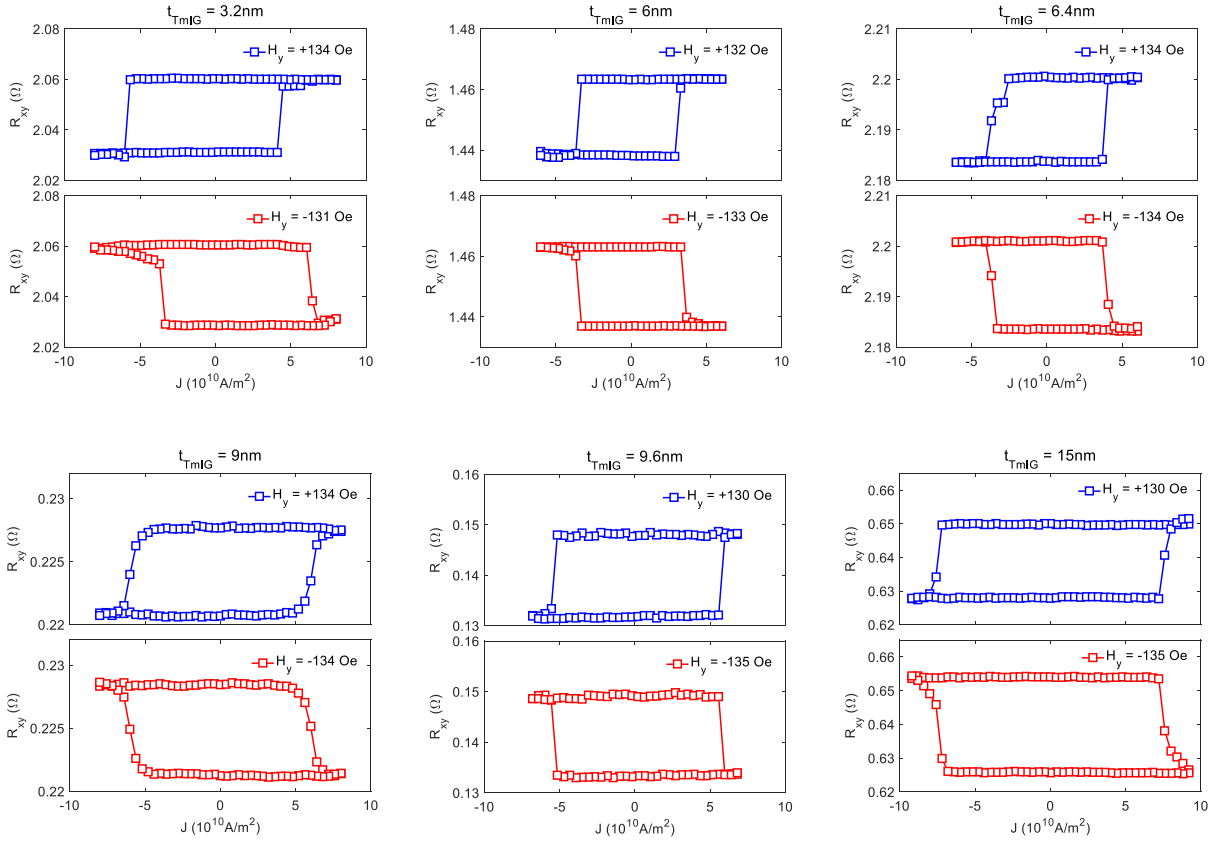

Figure 3-6 Current-induced magnetization switching in W/TmIG with t_{TmIG} ranging from 3.2 nm to 15 nm

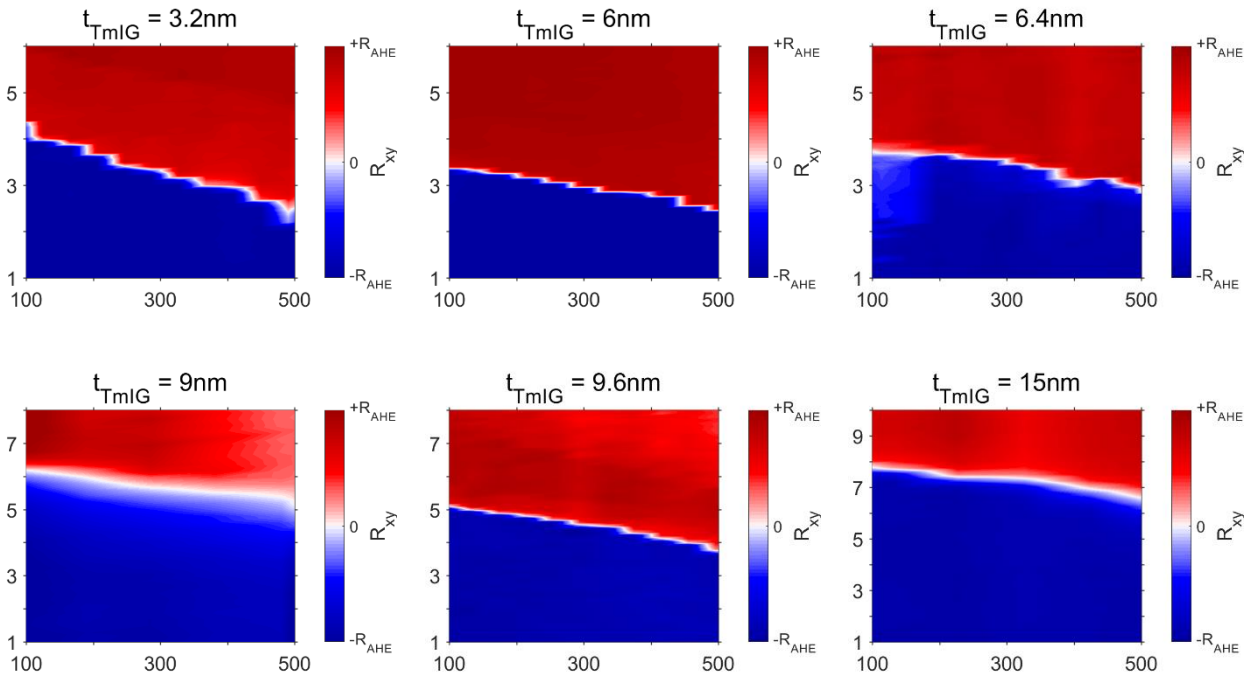

Figure 3-7 Switching phase diagram of W/TmIG with t_{TmIG} ranging from 3.2 nm to 15 nm

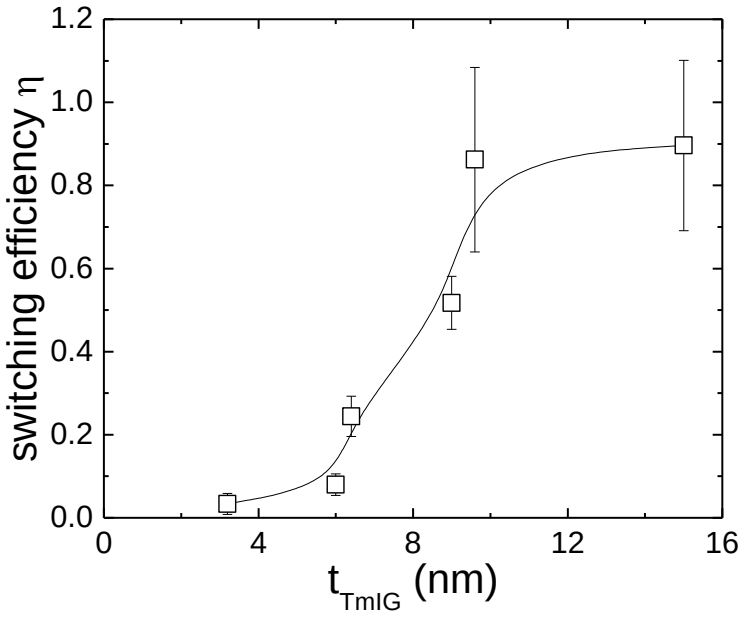

Figure 3-8 TmIG thickness dependent current switching efficiency, which is estimated from the depinning (coercive) field over switching current density in the zero-external field limit.

quantitatively compare the switching efficiency of W/TmIG devices with different t_{TmIG}, we define an effective switching efficiency as $\eta = \frac{2eM_S t_{TmIG} H_P}{\hbar J_{sw}(H_y \to 0)}$ [34], where H_P is the domain wall depinning field estimated from the coercive field and $J_{sw}(H_y \to 0)$ is the zero-field limit of current density in the switching phase diagram. This formula is applied when the CIMS is achieved through domain nucleation and domain wall motion in the Hall bar devices, and indeed the switching process is through domain wall nucleation and motion due to the large scale of our Hall bar devices. As shown in figure 3-7, the switching efficiency η increases with t_{TmIG}, and then saturated around 10nm. This result agrees well with the result in figure 3-2, which is self-consistent that that a larger SOT efficiency ξ_{DL} results in a larger switching efficiency η.

CHAPTER 5

CONCLUSION

1.1. Summary

In this thesis, based on the magneto transport measurement, we studied the thickness dependent SOT efficiency of the thulium iron garnet (TmIG)/ tungsten (W) bilayer structure, using both second harmonic method and loop-shift method. We further achieved SOT magnetic switching the TmIG/W bilayer with different TmIG thickness. The switching current density is as low as 7.5×10^{10} A/m^2 for the W (5 nm)/TmIG (15 nm). It is revealed that, both SOT efficiency and switching efficiency increase with the saturation magnetic momentum, which is is in consistence with the theoretical proposed M_S-effect. We also developed an atomic spin model to numerically simulate the fast domain wall motion in ferrimagnetic material near its angular compensation temperature, aiming to discuss the possibility for high speed magnetization switching is TmIG/W bilayer. This finding shed light on the understanding of SOT in MIs and promote the development of MI-based low-power high-speed spintronics

1.2. Future Work

The future work would be finishing the simulation of fast domain wall motion in ferrimagnet near angular momentum compensation point, and then carry out new experiment to study the ultra-fast pulse switching of TmIG/W bilayers.

REFERENCES

[1] Waldrop, M. M. (2016). The chips are down for Moore's law. Nature News, 530(7589), 144.

[2] Mack, C. A. (2011). Fifty years of Moore's law. IEEE Transactions on semiconductor manufacturing, 24(2), 202-207.

[3] Dreslinski, R. G., Wieckowski, M., Blaauw, D., Sylvester, D., & Mudge, T. (2010). Near-threshold computing: Reclaiming moore's law through energy efficient integrated circuits. Proceedings of the IEEE, 98(2), 253-266.

[4] Cavin, R. K., Lugli, P., & Zhirnov, V. V. (2012). Science and engineering beyond Moore's law. Proceedings of the IEEE, 100(Special Centennial Issue), 1720-1749.

[5] Baibich, M. N., Broto, J. M., Fert, A., Van Dau, F. N., Petroff, F., Etienne, P., ... & Chazelas, J. (1988). Giant magnetoresistance of (001) Fe/(001) Cr magnetic superlattices. Physical review letters, 61(21), 2472.

[6] Mathur, H. (1991). Thomas precession, spin-orbit interaction, and Berry's phase. Physical review letters, 67(24), 3325

[7] Marian, C. M. (2001). Spin-orbit coupling in molecules. Reviews in computational chemistry, 17, 99-204.

[8] Winkler, R., Papadakis, S. J., De Poortere, E. P., & Shayegan, M. (2003). Spin-Orbit Coupling in Two-Dimensional Electron and Hole Systems (Vol. 41, p. 211). Springer.

[9] Dresselhaus, G. (1955). Spin-orbit coupling effects in zinc blende structures. Physical Review, 100(2), 580.

[10] Bychkov, Y. A., & Rashba, E. I. (1984). Oscillatory effects and the magnetic susceptibility of carriers in inversion layers. Journal of physics C: Solid state physics, 17(33), 6039.

[11] Kittel, C., McEuen, P., & McEuen, P. (1996). Introduction to solid state physics (Vol. 8, pp. 323-324). New York: Wiley.

[12] Zhang, S., & Li, Z. (2004). Roles of nonequilibrium conduction electrons on the magnetization dynamics of ferromagnets. Physical Review Letters, 93(12), 127204.

[13] Brataas, A., Tserkovnyak, Y., & Bauer, G. E. (2008). Scattering theory of Gilbert damping. Physical review letters, 101(3), 037207.

[14] Brataas, A., Kent, A. D., & Ohno, H. (2012). Current-induced torques in magnetic materials. Nature materials, 11(5), 372.

[15] Ralph, D. C., & Stiles, M. D. (2008). Spin transfer torques. Journal of Magnetism and Magnetic

Materials, 320(7), 1190-1216.

[16] Wang, K. L., Alzate, J. G., & Amiri, P. K. (2013). Low-power non-volatile spintronic memory: STT-RAM and beyond. Journal of Physics D: Applied Physics, 46(7), 074003.

[17] Prenat, G., Jabeur, K., Di Pendina, G., Boulle, O., & Gaudin, G. (2015). Beyond STT-MRAM, spin orbit torque RAM SOT-MRAM for high speed and high reliability applications. In Spintronics-based Computing (pp. 145-157). Springer, Cham.

[18] Qiu, X., Narayanapillai, K., Wu, Y., Deorani, P., Yang, D. H., Noh, W. S., ... & Yang, H. (2015). Spin–orbit-torque engineering via oxygen manipulation. Nature nanotechnology, 10(4), 333.

[19] Kato, Y. K., Myers, R. C., Gossard, A. C., & Awschalom, D. D. (2004). Observation of the spin Hall effect in semiconductors. science, 306(5703), 1910-1913.

[20] Stern, N. P., Ghosh, S., Xiang, G., Zhu, M., Samarth, N., & Awschalom, D. D. (2006). Current-induced polarization and the spin Hall effect at room temperature. Physical review letters, 97(12), 126603.

[21] Kimura, T., Otani, Y., Sato, T., Takahashi, S., & Maekawa, S. (2007). Room-temperature reversible spin Hall effect. Physical review letters, 98(15), 156601.

[22] Miron, I. M., Garello, K., Gaudin, G., Zermatten, P. J., Costache, M. V., Auffret, S., ... & Gambardella, P. (2011). Perpendicular switching of a single ferromagnetic layer induced by in-plane current injection. Nature, 476(7359), 189.

[23] Nagaosa, N., Sinova, J., Onoda, S., MacDonald, A. H., & Ong, N. P. (2010). Anomalous hall effect. Reviews of modern physics, 82(2), 1539.

[24] Geprägs, S., Kehlberger, A., Della Coletta, F., Qiu, Z., Guo, E. J., Schulz, T., ... & Huebl, H. (2016). Origin of the spin Seebeck effect in compensated ferrimagnets. Nature communications, 7, 10452.

[25] Tang, C., Sellappan, P., Liu, Y., Xu, Y., Garay, J. E., & Shi, J. (2016). Anomalous Hall hysteresis in T m 3 F e 5 O 12/Pt with strain-induced perpendicular magnetic anisotropy. Physical Review B, 94(14), 140403.

[26] Bender, S. A., & Tserkovnyak, Y. (2015). Interfacial spin and heat transfer between metals and magnetic insulators. Physical Review B, 91(14), 140402.

[27] Nakayama, H., Althammer, M., Chen, Y. T., Uchida, K., Kajiwara, Y., Kikuchi, D., ... & Gross, R. (2013). Spin Hall magnetoresistance induced by a nonequilibrium proximity effect. Physical review letters, 110(20), 206601.

[28] Chen, Y. T., Takahashi, S., Nakayama, H., Althammer, M., Goennenwein, S. T., Saitoh, E., & Bauer, G. E. (2013). Theory of spin Hall magnetoresistance. Physical Review B, 87(14), 144411.

[29] Shao, Q., Yu, G., Lan, Y. W., Shi, Y., Li, M. Y., Zheng, C., ... & Wang, K. L. (2016). Strong Rashba-Edelstein Effect-Induced Spin–Orbit Torques in Monolayer Transition Metal Dichalcogenide/Ferromagnet Bilayers. Nano letters, 16(12), 7514-7520.

[30] Liu, L., Pai, C. F., Li, Y., Tseng, H. W., Ralph, D. C., & Buhrman, R. A. (2012). Spin-torque switching with the giant spin Hall effect of tantalum. Science, 336(6081), 555-558.

[31] Bender, S. A., & Tserkovnyak, Y. (2015). Interfacial spin and heat transfer between metals and magnetic insulators. Physical Review B, 91(14), 140402.

[32] Pai, C. F., Mann, M., Tan, A. J., & Beach, G. S. (2016). Determination of spin torque efficiencies in heterostructures with perpendicular magnetic anisotropy. Physical Review B, 93(14), 144409.

[33] Avci, C. O., Quindeau, A., Pai, C. F., Mann, M., Caretta, L., Tang, A. S., ... & Beach, G. S. (2017). Current-induced switching in a magnetic insulator. Nature materials, 16(3), 309.

[34] Lee, O. J., Liu, L. Q., Pai, C. F., Li, Y., Tseng, H. W., Gowtham, P. G., ... & Buhrman, R. A. (2014). Central role of domain wall depinning for perpendicular magnetization switching driven by spin torque from the spin Hall effect. Physical Review B, 89(2), 024418.